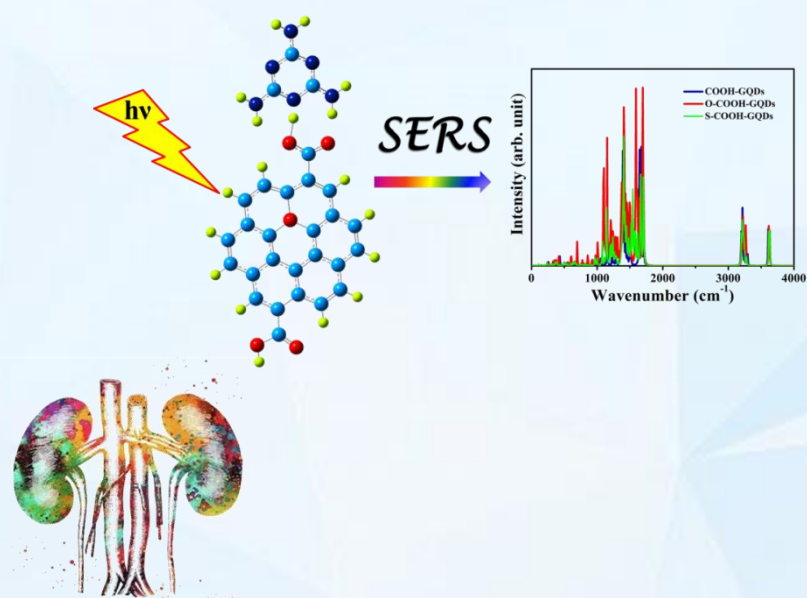


Chapter 6

Utilization of doped and functionalized GQDs for ultrasensitive detection of catastrophic melamine: A new SERS platform



6.1 Introduction

A lethal scandal in china has become a haunting calamity in the world even after ten years because of the death of six infants along with ~3,00,000 illnesses [1]. This catastrophe is a result of addition of chemical compound known as “melamine” in toddler’s milk powder to synthetically increase the protein content [1]. Melamine having $C_3H_6N_6$ molecular formula is an organic compound consisting ample of nitrogen atoms [2] and has application as a chemical agent in industries in plastics, kitchen equipment, fertilizer manufacturing, adhesives, coatings etc. [3-5]. The standard adequate consumption of melamine is 0.63 mg/kg barely [6]. However, on the basis of United States Food and Drug Administration (FDA), the melamine quantity in milk powder was noticed to be in critically considerable setting of 2560 mg/kg. Besides this, melamine utilized in pet foods also led to hundreds of deaths in dogs and cats in USA in 2007. The melamine intake causes bladder and kidney stones leading to kidney breakdown in humans [7,8]. Hence, it is important to hunt down and manage the quantity of melamine. Limited investigations were reported for systematic detection of melamine [9-12]. For the detection of melamine these investigations comprise methods like liquid chromatography with tandem mass spectrometry (LC-MS-MS), mass spectrometry (MS) and low temperature plasma (LTP) ionization with MS-MS [13-15]. However, they are dreary which demand pre-treatment of specimen such as extraction, pre-concentration and derivatization. On the other hand, Raman spectrum requires nominal or no sample preparation in providing “fingerprint-like” information without damaging any samples [16]. Despite precision and effective recognition of molecules, there are still the hindrances for tiny molecules resulting in feeble signals of Raman spectroscopy. Surface enhanced Raman spectroscopy (SERS) contributed in enhancing those feeble Raman signals even in case of single molecule [17-22]. After the introduction of SERS, the exploration for functional substrates comprising greater sensitivity, replicability and consistency were started. Noble and transition metals like silver, gold, copper, silicon, palladium etc. were conventionally employed as substrates [23,24]. However, novel substrates are developing concern about biocompatibility, stability, expenditures and sustainable nature. The well-known graphene [25] presents remarkable Raman scattering characteristics in comparison with noble metals because of its reliable chemical stability, adsorptivity and biocompatibility together with exceptional electronic and phonon properties [26]. The substrate made up of

graphene to enhance Raman scattering is known as “Graphene-enhanced Raman scattering (GERS)”. Bringing together graphene with metal substrates consequently increases its Raman signals [27]. Different allotropes of graphene such as graphene oxide (GO), aged and nanomesh graphene and graphene quantum dots (GQDs) were investigated which presented their role for SERS applications [28-32]. The increment is because of the chemical effects together with its ability to transmit ample of visible wavelength [33]. Raman signals in graphene are found to be increased by 2 to 17-fold (of phthalocyanine) in comparison with SiO₂/Si substrate which is even beneath the metal substrates [34]. GQDs have gained much attention in this field attributed to quantum confinement and edge effects. The large surface area and exposed edges of these quantum dots provide easy adsorption of targeted molecules [33]. GQDs possess noteworthy signals of SERS to find target molecules attributed to their effective photo-electronic properties [26,33,35]. Furthermore, it is notable that the functionalization of GQDs modifies their properties [36-37]. Motivated by the above facts, present work is studied with two different GQDs: (i) oxygen (O) and sulphur (S) doped GQDs [38], and (ii) epoxy, hydroxyl, and carboxyl groups functionalized GQD with the aim to sense melamine [39]. The geometrical, electronic and vibrational characteristics of melamine over these two GQDs were studied to identify superior substrate for the detection of melamine.

6.2 Computational Details

Density functional theory based on first principles calculation is utilized to perform calculations to find geometrical, electronic and vibrational properties via Gaussian09 software [40]. Minimum energy is precisely predicted through hybrid functional B3LYP, which is the blend of Hartree-Fock exchange and Becke exchange functional (Becke three parameter). The B3LYP [41-42] incorporates non-local correlation functional from Lee, Yang and Parr (LYP) along with local correlation from Vosko, Wilk, and Nusair functional (VWN III) [43]. The 6-31G basis set was used comprising orbitals of inner-shell provided through six Gaussian functions along with four Gaussians consisting split-valence set for valence orbitals with subsets of three and one.

Doped GQDs

To perform detection of melamine over oxygen doped GQD (O-GQD) sulphur doped GQD (S-GQD), structural optimization of their pristine forms along with adsorption were done. The

surface-on framework, in which, melamine was positioned parallel to the surface of O-GQD and S-GQD, was adopted for the interaction. Melamine over O-GQD (Mel-O-GQD) and melamine over S-GQD (Mel-S-GQD) in their optimization process were relaxed together until the gradient forces levels 0.00045 Hartree threshold value. The diagonalization of mass weighted Hessian matrix was used to evaluate the vibrational modes. The adsorption energy (E_{ad}) of Mel-O-GQD and Mel-S-GQD is evaluated through equation:

$$E_{ad} = E_{Melamine+O/S-GQD} - (E_{Melamine} + E_{O/S-GQD}) \quad (6.1)$$

here $E_{Melamine+O/S-GQD}$ represents melamine optimized total energy over O-GQD and S-GQD, $E_{O/S-GQD}$ represents individual optimization energy of oxygen doped GQD and sulphur doped GQD. $E_{Melamine}$ represents pristine melamine's optimized energy. The minus sign of E_{ad} from equation (6.1) depicts a stable adsorption complex over both GQD systems.

Functionalized GQDs

In the next, detection of melamine is performed over GQD functionalized with epoxy, hydroxyl, and carboxyl groups, naming it as “*f*-GQD”. Along with 6-31G basis set, diffusion (d) and polarization (p) functions were also employed. To compare, melamine is placed over both pristine GQD and *f*-GQD to check the interaction mechanism. The E_{ad} is defined using equation:

$$E_{ad} = E_{Melamine+GQD/f-GQD} - (E_{Melamine} + E_{GQD/f-GQD}) \quad (6.2)$$

Here, $E_{Melamine+GQD/f-GQD}$ depicts melamine and *f*-GQD system's total optimized energy, $E_{GQD/f-GQD}$ and $E_{Melamine}$ represents energy of separate GQD/*f*-GQD and melamine respectively.

6.3 Results and Discussions

6.3.1 Doped GQDs

6.3.1.1 Structural and Binding Interaction

In order to explore geometrical properties, oxygen doped GQD and sulphur doped GQD were investigated before and after the adsorption of melamine. The optimized structures of oxygen doped GQD and sulphur doped GQD are presented in Fig. 6.1. GQDs are minute fractions of 2D graphene inside of which atoms of carbon are compacted in hexagonal rings.

The O and S atoms were switched with the sites beyond electronegative atom (oxygen) of GQD to assure minimal deformation. Consequently, the most appropriate sites for substitution would be the hexagonal ring of carbon atoms (C3, C6, C7, C8, C41 and C42).

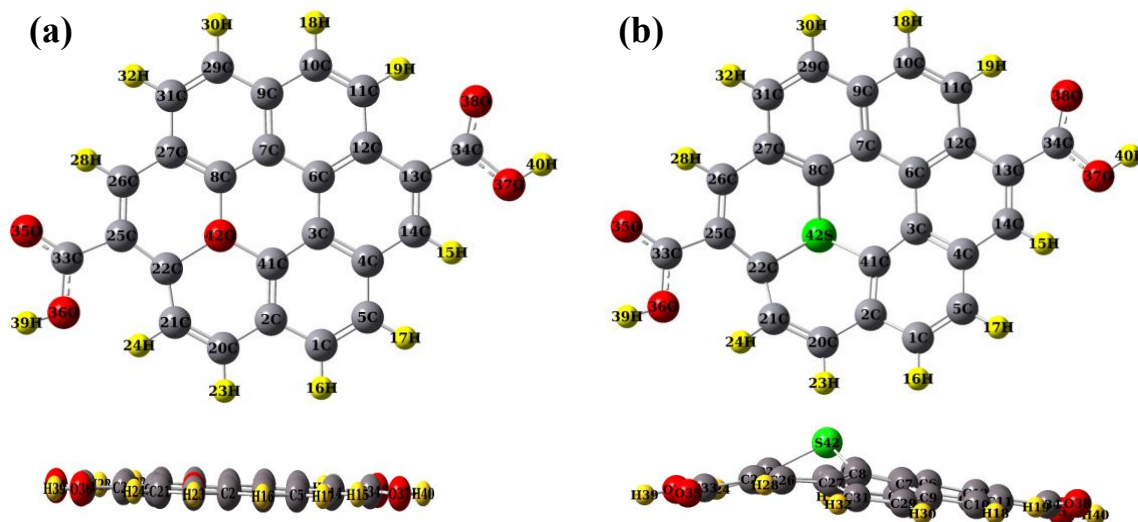


Figure 6.1: Optimized geometries of GQDs with (a) oxygen doped GQD and (b) sulphur doped GQD.

Considering that the carbon atoms comprise similar surrounding and coordination number, carbon atom labeled as 42C (Fig. 6.1) was selected for substitution. The selection of site also assists the range of melamine. Additionally, the size of both GQDs is 1.36 nm, which is suitable as a substrate for melamine adsorption of size 0.63 nm. Accordingly, an individual melamine is adsorbed over single unit of oxygen doped GQD and sulphur doped GQD. Further, the doping percentage is 3.8% for oxygen and sulphur inclusion. In GQDs, the C-C atoms bond length is ~ 1.42 Å [37,44], while after the doping of oxygen, the bond length is altered among C-O-C atoms due to the local distortion as presented in Fig. 6.1(a). The bond length is 1.622 Å for C-42O, 1.52 Å for 41C-42O and 1.48 Å for 8C-42O atoms, which is in accordance with other reported work [45] and greater than pristine GQDs. The attained bond angles are also in agreement with reported studies [46-47] with values of 120.1° for 22C-42O-41C, 118.5° for 41C-42O-8C and 121.2° for 8C-42O-22C. The structural investigation presents that the plane sp^2 configuration and delocalization of π -electron are conserved in O-GQD.

Moreover, in S-GQD, for atom 22C-42S, the bond length is 1.89 Å. In 41C-42S, the bond length is 1.84 Å and in 8C-42S, the bond length is 1.83 Å, leading in additional geometrical deformation in comparison with O-GQD (uplift of sulphur from the plane of GQD (Fig. 6.1(b)). The pyramid like structure is due to large radius of S atom converting sp^2 to sp^3 hybridized carbon and is in agreement with other work [48]. The identification of binding interactions of melamine, adsorption energies are evaluated using equation (6.1).

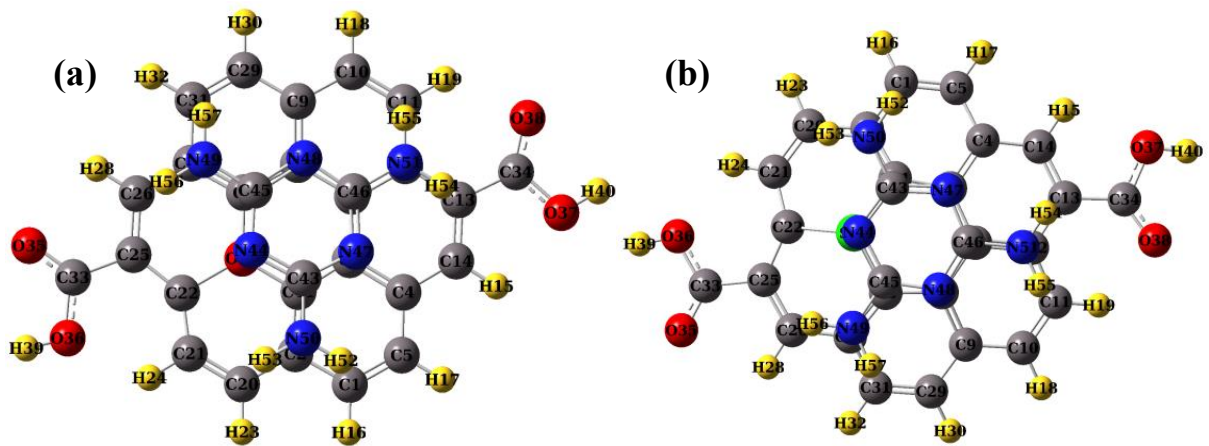


Figure 6.2: Initial geometries of (a) Mel-O-GQD and (b) Mel-S-GQD.

Figure 6.2 presents the primary configuration of Mel-O-GQD and Mel-S-GQD. After the geometry optimization, in case of O-GQD, melamine tends to adsorb at the boundary near carboxyl group, whereas, in S-GQD, melamine reorients itself on S-GQD near the sulphur doping. Following geometry optimization, adsorption energy is calculated through equation (6.1). The E_{ad} of melamine is -1.182 eV and -0.15 eV for O-GQD and S-GQD respectively, presented in Table 6.1. The O-GQD shows greater E_{ad} attributed to its superior electronegative nature than sulphur. The E_{ad} is even greater than melamine adsorbed over graphene with LDA functional [12]. To clearly depict the adsorption mechanism, electronic properties were also analyzed.

Table 6.1: Computed HOMO and LUMO energies, HOMO-LUMO gap (E_g) and adsorption energy (E_{ad}) of all systems.

System	E_{HOMO} (eV)	E_{LUMO} (eV)	E_g (eV)	E_{ad} (eV)
Melamine	-6.189	0.507	6.696	-
O-GQD	-4.052	-2.478	1.57	-
S-GQD	-4.637	-2.479	2.15	-
Mel-O-GQD	-3.599	-1.941	1.658	-1.182
Mel-S-GQD	-4.689	-2.5	2.189	-0.15

6.3.1.2 Electronic Properties

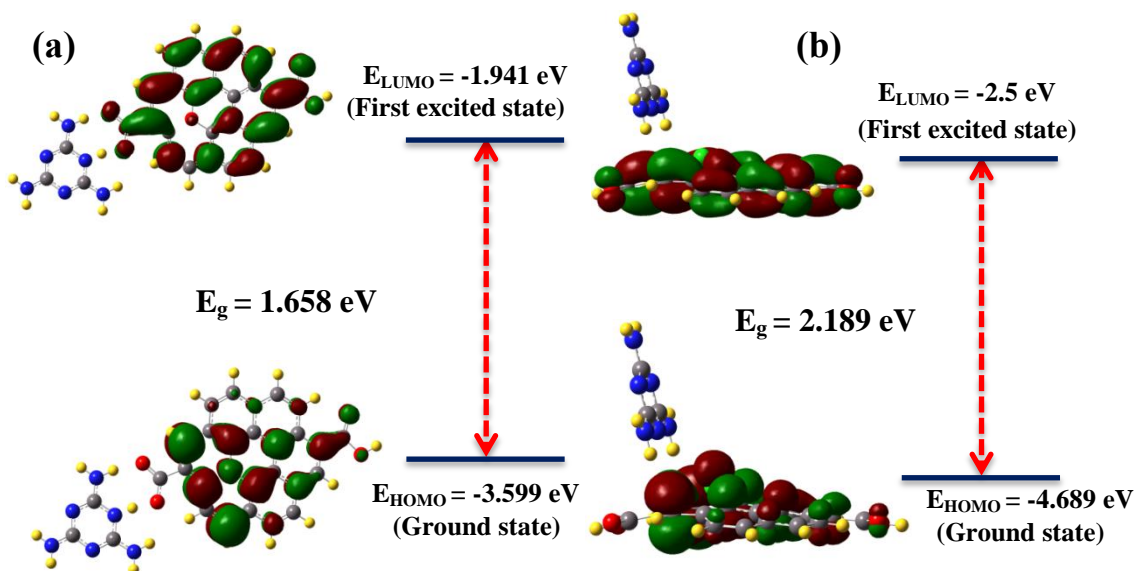


Figure 6.3: HOMO-LUMO surfaces of (a) Mel-O-GQD and (b) Mel-S-GQD.

The highest occupied molecular orbitals (HOMO) and lowest unoccupied molecular orbitals (LUMO) were studied to comprehend above interaction mechanism of melamine over O-GQD and S-GQD and are presented in Fig. 6.3. The donor nature of electrons is depicted through HOMO, while, the acceptor nature is depicted through LUMO. The HOMO and LUMO determine the process of adsorption mechanism between adsorbate and adsorbent. The delocalization of π -bonds in Fig. 6.3 (a-b) is presented through the distribution of HOMO and

LUMO on O-GQD and S-GQD. Though, the doping further weakens it [48]. The magnitude of HOMO-LUMO gaps (E_g) is given in Table 6.1. The positive and negative orbitals of HOMO-LUMO are presented through red and green colors. The position of HOMO-LUMO energies deviates subsequent to melamine adsorption. The E_g is 1.658 for Mel-O-GQD and 2.189 eV for Mel-S-GQD. The E_g is evaluated to study the charge transfer among systems leading to the modification in their chemical reactivity. It is found that there is no change in E_g of Mel-S-GQD, however, E_g increases from 1.57 to 1.658 ($\approx 9\%$) in Mel-O-GQD depicting noteworthy charge transfer. Besides, the molecular electrostatic potential (MESP) is also investigated to comprehend the link between geometries and chemical activity of all considered systems and presented them in Fig. 6.4.

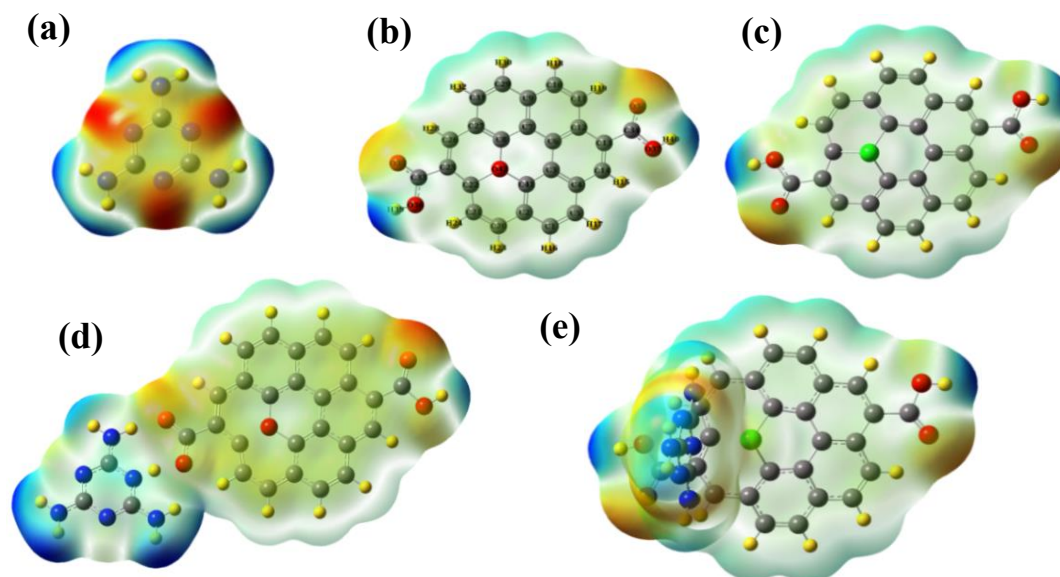


Figure 6.4: MESP surfaces of (a) pristine melamine (b) O-GQD (c) S-GQD (d) Mel-O-GQD and (e) Mel-S-GQD.

Traditionally, red region presents electrophilic part with additional electrons while blue region presents nucleophilic part with lack of electrons. Hence, MESP carrying positively charged particles will bond intensely is depicted through red region and contrariwise for blue one. The aforementioned demonstrates the strong binding of -1.182 eV among melamine (red region) and O-GQD (blue part along boundaries) presented in Fig. 6.4(d).

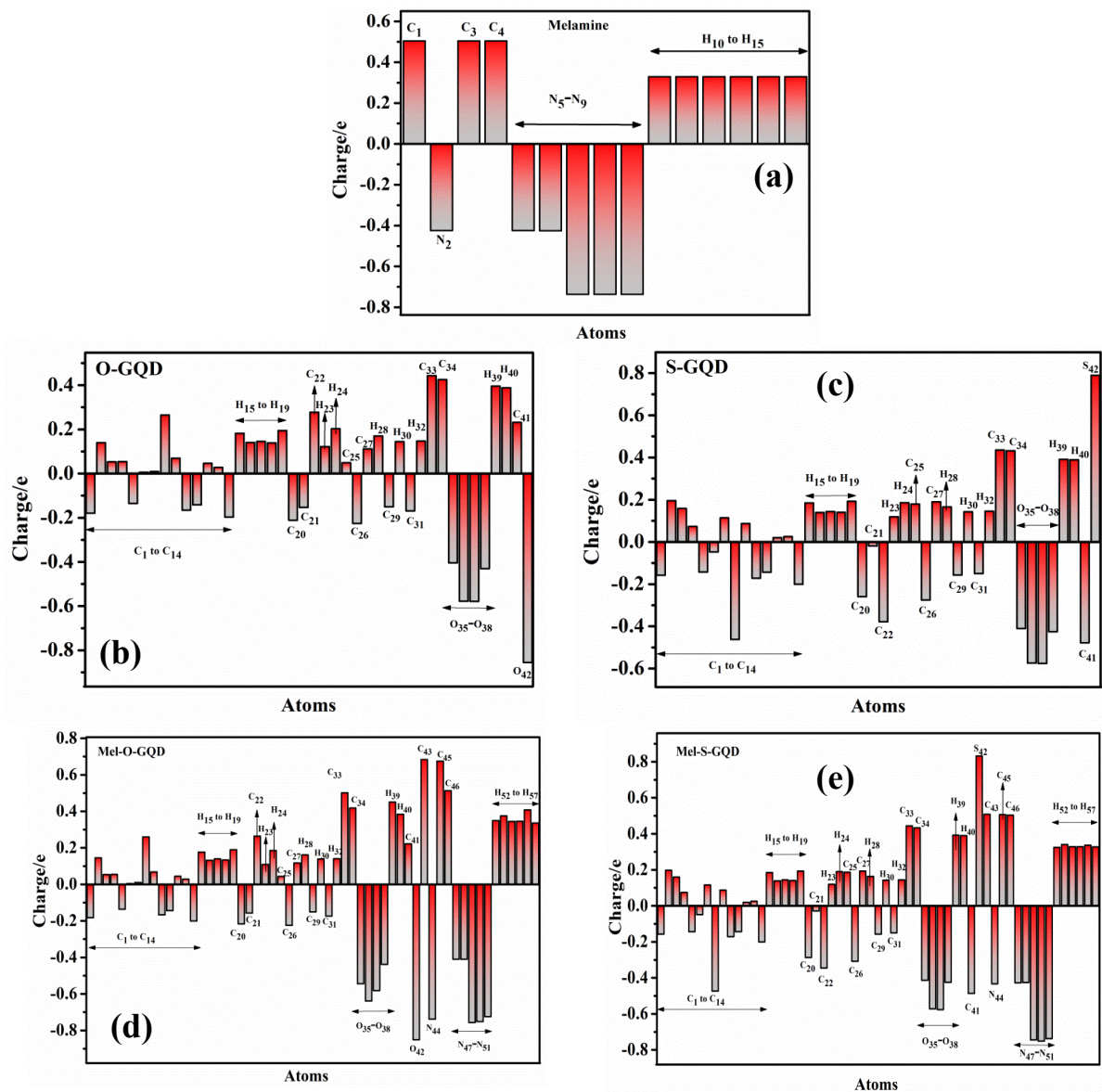


Figure 6.5: MPA of (a) pristine melamine (b) O-GQD (c) S-GQD (d) Mel-O-GQD and (e) Mel-S-GQD.

The Mulliken population analysis (MPA) is also explored as charge distribution comprises important impact on vibrational properties. MPA graphs of melamine, Mel-O-GQD and Mel-S-GQD are presented in Fig. 6.5. Graphs show that carbon atom bears positive and negative values of charges together, whereas, hydrogen atom bears only positive values of charges. In Mel-O-GQD, oxygen acquires charges arising out of melamine molecule (Fig. 6.5(b-d)). The fewer

charges are transposed in Mel-S-GQD due to low E_{ad} . The MPA of studied systems provides a platform for present calculation on chemical enhancement effects.

6.3.1.3 SERS Mechanism of Melamine over doped Graphene Quantum Dots

With the aim to investigate melamine detection, DFT calculations have been done to attain SERS chemical enhancement characteristics of Mel-O-GQD and Mel-S-GQD. The spectra of Raman and SERS of all considered systems are depicted in Fig 6.6. The graph is shown in twofolds ranging from (a) 200 cm^{-1} to 800 cm^{-1} and (b) 1000 cm^{-1} to 1600 cm^{-1} to systematically examine specific melamine peaks. The computed Raman signal is determined by strong peak obtained at 688 cm^{-1} which is analogous with other reported theoretical and experimental works [9-11,49].

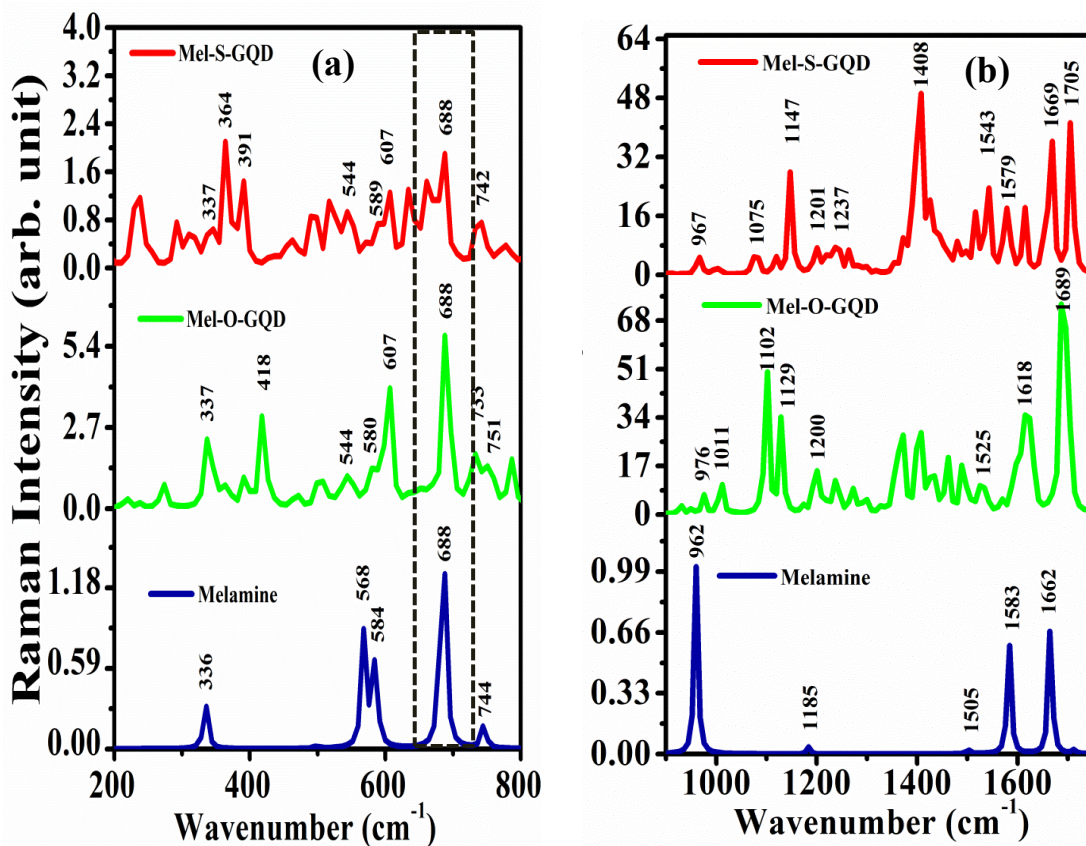


Figure 6.6: Theoretical Raman spectra of melamine, Mel-O-GQD and Mel-S-GQD ranging between (a) 200 cm^{-1} to 800 cm^{-1} and (b) 1000 cm^{-1} to 1600 cm^{-1} .

Table 6.2: Calculated Raman spectral data and vibrational assignments of pristine melamine, Mel-O-GQD and Mel-S-GQD.

Calculated Wavenumber (cm ⁻¹)			Assignments
Melamine	Mel-O-GQD	Mel-S-GQD	
336	337	337	NH ₂ wagging
568	544	544	NH ₂ twisting
584	580	589	C-N-C bending and NH ₂ twisting
688	688	688	Ring breathing
744	733	742	C-N-C bending (out-of-plane) and NH ₂ twisting
962	976	967	C-N-C bending
1505	1507	1507	C-N-C stretching (in plane)
1583	1597	1579	N-C-N bending (out-of-plane) and NH ₂ wagging
1662	1689	1669	N-C-N bending and NH ₂ bending

Experimentally, the peak obtained at ~688 cm⁻¹ is considered a characteristic peak for melamine molecule [11,49] which is specified as ring breathing vibration mode and is in agreement with previous published study [10]. The additional peaks of melamine are found at 336 cm⁻¹, 568 cm⁻¹, 584 cm⁻¹, 744 cm⁻¹, 962 cm⁻¹, 1185 cm⁻¹, 1505 cm⁻¹, 1583 cm⁻¹ and 1662 cm⁻¹. These are tabulated in Table 6.2 together with vibrational modes of Mel-O-GQD and Mel-S-GQD. The strong 688 cm⁻¹ peak is employed for SERS investigation. The impact of O-GQD and S-GQD over melamine is studied using intensity of spectra and vibrational assignments.

It is found that in O-GQD melamine is interacted using nitrogen and hydrogen atom, while in S-GQD, it is adsorbed through NH₂ group and sulphur. Both Raman and SERS spectra are presented in Fig. 6.6. As observed from Figs. 6.3-6.5, modification in electronic properties results in the chemical enhancement and Raman signals. Table 6.3 shows the chemical enhancement factors (*EF*) determined through following equation:

$$EF = (I_{SERS}/N_{SERS})/(I_{Raman}/N_{Raman}) \quad (6.3)$$

where, I_{SERS} and N_{SERS} depict Raman signal intensity and amount of molecules involved in SERS. I_{Raman} and N_{Raman} depict intensity of Raman signal and amount of molecules in normal Raman. The intensity of characteristic peak of Raman spectra in melamine at 688 cm^{-1} is 1.282 which increases to 5.748 (348.4 %) in Mel-O-GQD SERS (Fig. 6.6). The intensity increases up to 1.898 (48%) in case of Mel-S-GQD SERS spectra. It is noteworthy that the increment in intensity of Raman peak in O-GQD is even higher than silver clusters being the substrate for melamine [10].

Table 6.3: Evaluated enhancement factor (EF) of Mel-O-GQD and Mel-S-GQD.

System	Enhancement factor (EF)
Mel-O-GQD	4.51
Mel-S-GQD	1.481

Addition of oxygen and sulphur in GQD leads to the enhancement of intensity in other peaks of melamine along with the characteristic peak. The red shift is observed in peaks of melamine (962 cm^{-1} and 1662 cm^{-1}) adsorbed over both GQDs. The EF of Mel-O-GQD and Mel-S-GQD calculated through equation (6.3) is 4.51 and 1.48 respectively. This large enhancement is attributed mainly to the addition of oxygen in graphene quantum dots defining the chemical enhancement mechanism of SERS.

6.4.1 Functionalized GQDs

6.4.1.1 Structural and Binding Interaction

The geometry optimization is performed at three sites such as hollow, bridge, and top to study melamine interaction on rectangular GQD. Hollow site is depicted as central hexagonal ring positioned at hollow site of GQD presented in Fig. 6.7 (a). The top site is defined as the placement of melamine's central hexagonal ring on top of GQD's carbon atom at 1.5 \AA distance (Fig. 6.7 (b)). It is kept across the mid of carbon-carbon bond (Fig. 6.7 (c)). The upper row in

Fig. 6.7 presents initial structures of melamine over GQD and lower row shows optimized structures of melamine and GQD.

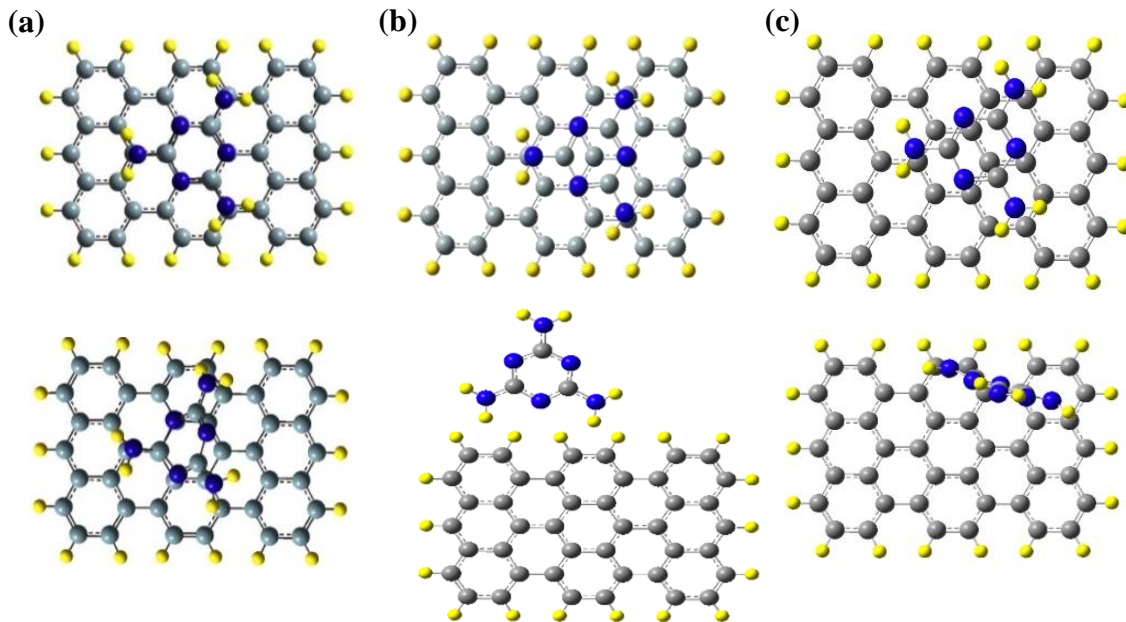


Figure 6.7: Initial and optimized geometries of (a) hollow melamine-GQD (b) top melamine-GQD and (c) bridge melamine-GQD.

Hollow site optimization shows that the carbon atom of GQD is elevated by nitrogen atom of melamine molecule, however, the remaining section of melamine is strongly repulsed resulting in the positive E_{ad} of 3.98 eV. This positive E_{ad} depicts the endothermic process and therefore impractical to adsorb. The E_{ad} of -0.16 eV is attained with melamine adsorption at top site. Melamine on bridge site of GQD presents negligible E_{ad} of -0.08 eV. All calculated E_{ad} are tabulated in Table 6.4.

Several studies propose the variation of geometries and electronic properties using functionalization [36-37]. Based on that, adsorption of melamine is also investigated on functionalized GQD (*f*-GQD). Three functional groups such as carboxyl, epoxy, and hydroxyl are joined to GQD assigning it as “functionalized-GQD (*f*-GQD)”.

Table 6.4: Calculated adsorption energy (E_{ad}) of melamine on GQD and *f*-GQD for all three sites.

System	Site	E_{ad} (eV)
GQD + melamine	Hollow	3.98
	Top	-0.16
	Bridge	-0.077
<i>f</i> -GQD + melamine	Hollow	-0.53
	Top	-0.53
	Bridge	-0.53

Figure 6.8 presents melamine adsorption over *f*-GQD (*f*-GQD-mel) subsequent to optimization of ground state. The similar E_{ad} of -0.53 eV is found for all hollow, top and bridge sites attributed to their equivalent geometrical properties. This homologous interaction in all three sites is the result of melamine interaction with hydroxyl group solely. Hence, results in the similar geometry configuration.

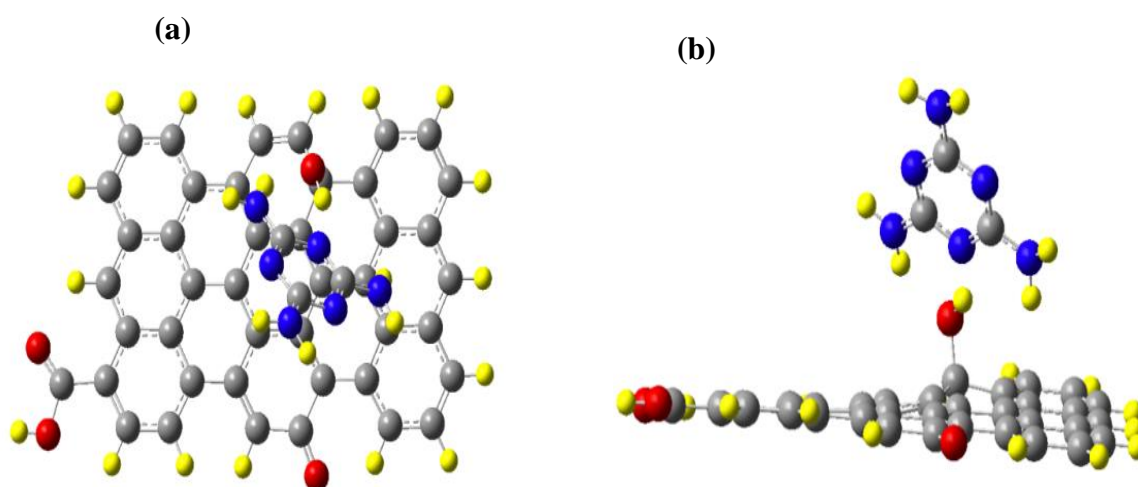


Figure 6.8: (a) Top view and (b) side view of optimized geometries of melamine over *f*-GQDs.

Further, due to the greater E_{ad} (three times) in *f*-GQD-mel as compared to pristine form, we have explored electronic and SERS properties of *f*-GQD-mel only.

6.4.1.2 Electronic Properties

The HOMO and LUMO together with E_g are explored to study the electronic properties. The chemical as well as kinetic stability of particular molecule is determined through the energy gap (E_g) between HOMO and LUMO [50]. Figure 6.9 shows HOMO, LUMO and E_g of melamine and *f*-GQD-mel.

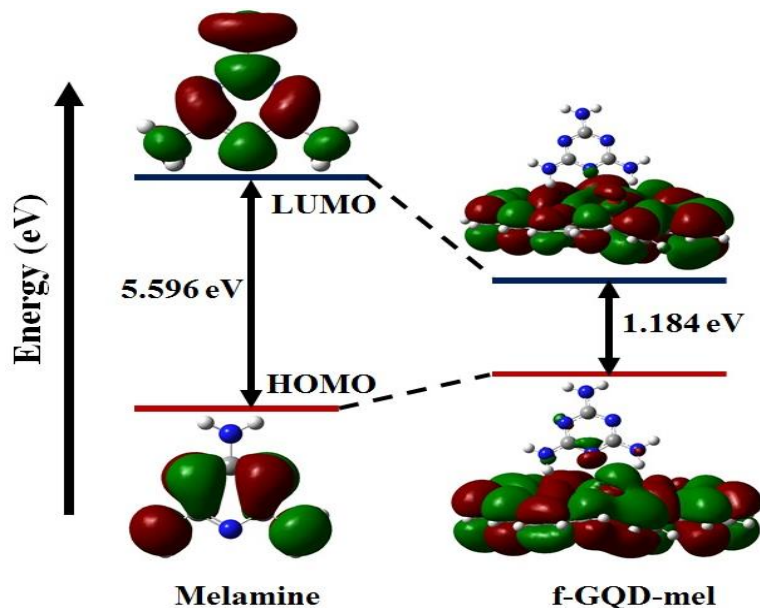


Figure 6.9: HOMO-LUMO levels of melamine and melamine over *f*-GQD.

The HOMO of melamine is confined to its C–N–C ring and two NH_2 groups, whereas, LUMO is localized on entire melamine as shown in Fig. 6.9. This orbital localization of melamine presents good agreement with other reported work [10]. In case of *f*-GQD-mel, minor HOMO is localized in the vicinity of nitrogen adjacent to functional group due to physisorption. The E_g of melamine decreases to 1.184 eV in case of *f*-GQD-mel. This decrease describes strong interaction along with charge transfer among adsorbate and adsorbent. It is noticeable that the positive charge of hydrogen (0.28) enhances to 0.34 when interacts with nitrogen atom of melamine molecule resulting in more negative charge of nitrogen atom in *f*-GQD. This will lead to the strong interaction, charge transfer and high chemical enhancement between melamine and *f*-GQD and further significantly modify SERS effect. This large decrement of E_g is greater as compared to earlier reported melamine over silver nanoclusters (0.10 eV) [10].

6.4.1.3 SERS Mechanism of Melamine over functionalized Graphene Quantum Dots

The calculated Raman spectra for pristine melamine and *f*-GQD-mel are depicted in Fig 6.10. The ring breathing vibrational mode of melamine is observed at 680 cm^{-1} . Additionally, the peak at 584 cm^{-1} shows bending of C–N–C and twisting of NH_2 group. Peak 736 cm^{-1} produces out-of-plane vibrations. These three 584 , 680 , and 736 cm^{-1} peaks of melamine comprise difference of 10 cm^{-1} only with present experimental results [10] providing consistency of present work. The Raman spectra of *f*-GQD-mel are also evaluated in order to understand effect of SERS on melamine. Here, it is noteworthy that all three adsorption sites provide similar E_{ad} with similar structural properties which will result in similar Raman spectra. Hence, only one site is studied for SERS.

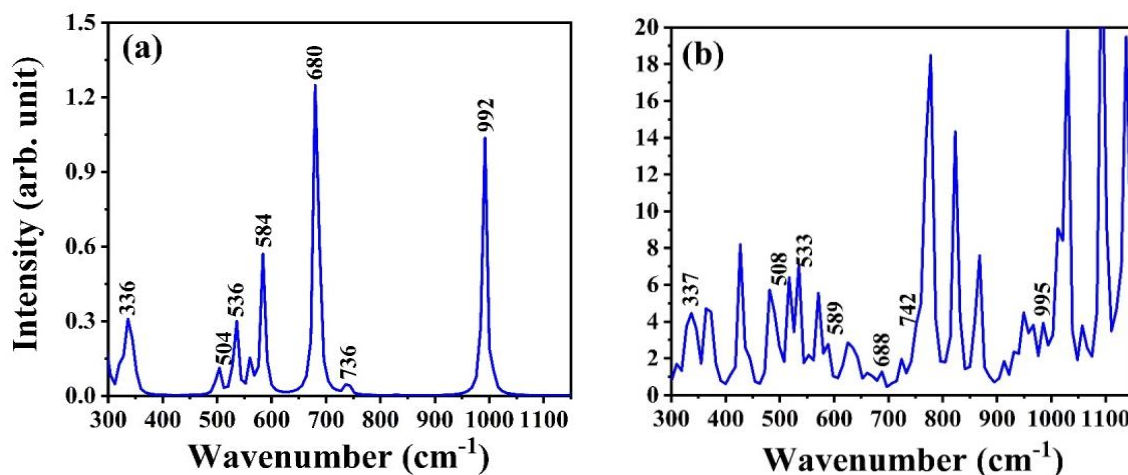


Figure 6.10: Plot of Raman spectra of (a) pristine melamine and (b) SERS of *f*-GQD-mel.

The melamine and *f*-GQD interaction is illustrated through peak shift of melamine from 680 to 685 cm^{-1} , 736 to 742 cm^{-1} . Vibrational modes of pristine melamine and *f*-GQD-mel are given in Table 6.5. The efficiency of SERS is defined through enhancement factor (EF) of Raman signals. The EF is evaluated through Eq. (6.3) and is presented in Table 6.5. The peak intensity of 736 cm^{-1} of melamine is 0.046 which increases to 1.843 with highest EF of 39.890 among all. The melamine peak 584 cm^{-1} enhances by 396% in *f*-GQD-mel. The EF of other peaks is also evaluated and mentioned in Table 6.5 for detail understanding.

Table 6.5. Evaluated Raman wavenumbers of melamine and *f*-GQD-mel in cm^{-1} together with *EF*.

Melamine	<i>f</i> -GQD-mel	<i>EF</i>
336	337	14.438
504	508	16.165
536	533	23.767
584	589	4.868
680	688	1.022
736	742	39.890
992	995	2.617

For instance, peak 536 cm^{-1} increases from 0.299 to 7.127 providing the *EF* of magnitude 23.766. The present study shows large increment in SERS of melamine when adsorbed over *f*-GQD allowing GQDs potential candidature for the detection of melamine.

6.5. Conclusions

In conclusion, with the aim of sensing and detection of organic compound melamine, density functional theory based first-principles calculations were performed with two models of graphene quantum dots (GQDs). The first model consists of oxygen and sulphur doped GQD and other model comprises epoxy, hydroxyl and carboxyl groups functionalized GQD. The structural, electronic and vibrational properties are studied for melamine, oxygen doped GQD, sulphur doped GQD along with melamine adsorption over these O/S-GQDs. To comprehend the efficacy of adsorption, adsorption energy (E_{ad}) is calculated for melamine adsorbed over oxygen doped GQD and sulphur doped GQD resulting in the physisorption. The HOMO-LUMO, MESP and MPA are also studied to show chemical enhancement mechanism in SERS. The detection of melamine was investigated through surface enhanced Raman scattering (SERS). It is found that melamine is more sensitive to the oxygen existence GQD as compared to sulphur contributing in the increment of Raman intensities. The ideal peak obtained at 688 cm^{-1} is increased by 348.4% with oxygen doped GQD substrate, however, it is increased by 48% with sulphur doped GQD as a substrate which is greater with respect to Ag substrate.

In the next study of melamine with pristine and *f*-GQD, structural, electronic, and vibrational properties were studied with hollow, bridge and top sites. The E_{ad} of -0.16 eV is found for melamine on hollow site of GQD which enhances to -0.53 eV for melamine over *f*-GQD. The Raman intensity of melamine is remarkably enhanced with the *f*-GQD as compared to GQD. Mathematically, SERS effect is evaluated through enhancement factor (*EF*). The *EF* is found to be 39.89, highest at peak value of 736 cm^{-1} . It is concluded that the evaluated enhancement factor in melamine over both doped and functionalized GQD is higher as compared to silver nanoclusters presenting their superiority for SERS detection of melamine.

Reference

1. C. A. Brown, K-S. Jeong, R. H. Poppenga, B. Puschner, D. M. Miller, A. E. Ellis, K-II Kang, S. Sum, A. M. Cistola, S. A. Brown, *J. Vet. Diagnostic Investig.* **19** (2007) 525–531.
2. R. Muñiz-Valencia, S. G. Ceballos-Magaña, D. Rosales-Martinez, R. Gonzalo-Lumbreras, A. Santos-Montes, A. Cubedo-Fernandez-Trapiella, R. C. Izquierdo-Hornillos, *Anal. Bioanal. Chem.* **392** (2008) 523–531.
3. X-M. Xu, Y-P. Ren, Y. Zhu, Z-X. Cai, J-L. Han, B-F. Huang, Y. Zhu, *Anal. Chim. Acta.* **650** (2009) 39–43.
4. X. Xu, J. Wang, K. Jiao, X. Yang, *Biosens. Bioelectron.* **24** (2009) 3153–3158.
5. L. J. Mauer, A. A. Chernyshova, A. Hiatt, A. Deering, R. Davis, *J. Agric. Food Chem.* **57** (2009) 3974–3980.
6. World Health Organization, WHO Guidelines for Safe Surgery: Safe surgery saves lives, 2009.
7. A. K-C. Hau, T. H. Kwan, P. K-T. Li, *J. Am. Soc. Nephrol.* **20** (2009) 245–250.
8. E. Chan, S.M. Griffiths, C.W. Chan, *Lancet.* **372** (2008) 1444–1445.
9. L. M. Chen, Y. N. Liu, *ACS Appl. Mater. Interfaces.* **3** (2011) 3091–3096.
10. N. T. T. An, D. Q. Dao, P. C. Nam, B. T. Huy, H. N. Tran, *Spectrochim. Acta - Part A Mol. Biomol. Spectrosc.* **169** (2016) 230–237.
11. J. Cheng, X. O. Su, Y. Yao, C. Han, S. Wang, Y. Zhao, *PLoS One.* **11** (2016) e0154402.
12. J. D. Wuest, A. Rochefort, *Chem. Commun.* **46** (2010) 2923–2925.

13. M. S. Filigenzi, E. R. Tor, R. H. Poppenga, L. A. Aston, B. Puschner, *Rapid Commun. Mass Spectrom.* **21** (2007) 4027–4032.
14. T. M. Vail, P. R. Jones, O. D. Sparkman, *J. Anal. Toxicol.* **31** (2007) 304–312.
15. G. Huang, Z. Ouyang, R. G. Cooks, *Chem. Commun.* **2009** (2008) 556–558.
16. C. R. Yonzon, C. L. Haynes, X. Zhang, J. T. Walsh, R. P. Van Duyne, *Anal. Chem.* **76** (2004) 78–85.
17. M. Fleischmann, P. J. Hendra, A. J. McQuillan, *Chem. Phys. Lett.* **26** (1974) 163–166.
18. M. G. Albrecht, J. A. Creighton, *J. Am. Chem. Soc.* **99** (1977) 5215–5217.
19. D. L. Jeanmaire, R. P. Van Duyne, *J. Electroanal. Chem. Interfacial Electrochem.* **84** (1977) 1–20.
20. E. Smith, G. Dent, *Modern Raman Spectroscopy - A Practical Approach*, (2004).
21. K. Kneipp, Y. Wang, H. Kneipp, L.T. Perelman, I. Itzkan, R. R. Dasari, M. S. Feld, *Phys. Rev. Lett.* **78** (1997) 1667–1670.
22. S. Nie, S. R. Emory, *Science* **275** (1997) 1102–1106.
23. B. Ren, G. K. Liu, X. B. Lian, Z. L. Yang, Z. Q. Tian, *Anal. Bioanal. Chem.* **388** (2007) 29–45.
24. M. Fan, G. F. S. Andrade, A. G. Brolo, *Anal. Chim. Acta.* **693** (2011) 7–25.
25. K. S. Novoselov, A. K. Geim, S. V. Morozov, D. Jiang, Y. Zhang, S. V. Dubonos, I. V. Grigorieva, A. A. Firsov, *Science* **306** (2004) 666–669.
26. W. Xu, N. Mao, J. Zhang, *Small* **9** (2013) 1206–1224.
27. M. S. Dresselhaus, Z. Liu, J. Xiao, H. Xu, X. Ling, J. Kong, W. Xu, J. Zhang, *Proc. Natl. Acad. Sci.* **109** (2012) 9281–9286.
28. S. Huh, J. Park, Y. S. Kim, K. S. Kim, B. H. Hong, J. M. Nam, *ACS Nano.* **5** (2011) 9799–9806.
29. X. Yu, H. Cai, W. Zhang, X. Li, N. Pan, Y. Luo, X. Wang, J. G. Hou, *ACS Nano.* **5** (2011) 952–958.
30. Y. Wang, Z. Ni, A. Li, Z. Zafar, Y. Zhang, Z. Ni, S. Qu, T. Qiu, T. Yu, Z. X. Shen, *Appl. Phys. Lett.* **99** (2011) 233103.

-
31. J. Liu, H. Cai, X. Yu, K. Zhang, X. Li, J. Li, N. Pan, Q. Shi, Y. Luo, X. Wang, *J. Phys. Chem. C* **116** (2012) 15741–15746.
 32. A. K. Geim, K. S. Novoselov, *Nat. Mater.* **6** (2007) 183–191.
 33. H. Cheng, Y. Zhao, Y. Fan, X. Xie, L. Qu, G. Shi, *ACS Nano*. **6** (2012) 2237–2244.
 34. X. Ling, L. Xie, Y. Fang, H. Xu, H. Zhang, J. Kong, M. S. Dresselhaus, J. Zhang, Z. Liu, *Nano Lett.* **10** (2010) 553-561.
 35. M. Bacon, S. J. Bradley, T. Nann, Graphene quantum dots, *Part. Part. Syst. Charact.* **31** (2014) 415-428.
 36. P. Tian, L. Tang, K. S. Teng, S. P. Lau, *Mater. Today Chem.* **10** (2018) 221–258.
 37. V. Sharma, N. N. Som, S. D. Dabhi, P. K. Jha, *ChemistrySelect* **3** (2018) 2390–2397.
 38. V. Sharma, N.N. Som, S.B. Pillai, P. K. Jha, *Spectrochim. Acta A* **224** (2020), 117352.
 39. V. Sharma, H. L. Kagdada, D. K. Singh, P. K. Jha, *In: Singh D., Das S., Materny A. (eds) Advances in Spectroscopy: Molecules to Materials. Springer Proceedings in Physics, vol 236. Springer, Singapore* (2019).
 40. M. J. Frisch, et al. Gaussian 09, Revision D.01, Gaussian Inc. (2013) 1-20.
 41. A. D. Becke, *Phys. Rev. A* **38** (1988) 3098-3100.
 42. C. Lee, W. Yang, R.G. Parr, *Phys. Rev. B* **37** (1988) 785-789.
 43. S. H. Vosko, L. Wilk, M. Nusair, *Can. J. Phys.* **58** (1980) 1200-1211.
 44. D. Raeyani, S. Shojaei, S. Ahmadi-Kandjani, *Superlattice. Microst.* **114** (2018) 321-330.
 45. J. Feng, H. Dong, L. Yu, L. Dong, *J. Mater. Chem. C* **5** (2017) 5984-5993.
 46. B. Wannoo, C. Tabtimsai, *Superlattice. Microst.* **67** (2014) 110-117.
 47. A. S. Rad, *Appl. Surf. Sci.* **357** (2015) 1217-1224.
 48. J. Feng, H. Dong, B. Pang, F. Shao, C. Zhang, L. Yu, L. Dong, *Phys. Chem. Chem. Phys.* **20** (2018) 15244-15252.
 49. Q. Cao, K. Yuan, J. Yu, J.J. Delaunay, R. Che, *J. Colloid Interface Sci.* **490** (2017) 23-28.
 50. K. Geetha, M. Umadevi, G.V. Sathe, P. Vanelle, T. Terme, O. Khoumeri, *Spectrochim. Acta A* **138** (2015) 113–119.